DNS OF TURBULENT FLOW IN AN OPEN CHANNEL WITH A LONGITUDINALLY RIDGED BOTTOM WALL

Fumiaki MURAMATSU
Department of Mechanical Engineering, Faculty of Science and Technology,
Science University of Tokyo, Noda-shi, Chiba-ken 278-8510
a7596163@rs.noda.sut.ac.jp

Hiroshi KAWAMURA
Department of Mechanical Engineering, Faculty of Science and Technology,
Science University of Tokyo, Noda-shi, Chiba-ken 278-8510
kawa@rs.noda.sut.ac.jp

ABSTRACT

A DNS of turbulent channel with a ridged bottom has been carried out to simulate the sand ribbons over the river bed. Two cases are considered; one is a ridged closed channel with ridged top and bottom walls and the other is the one with a ridged bottom and a free top surface. The latter case reproduces well the flow structure around the ridge in the actual river. A low speed streak over the ridge is captured by the conditional sampling and its structure is discussed.

INTRODUCTION

Turbulent flows over complex geometries are often encountered in environmental and engineering problems. For example, sediment is concentrated over a river bed to form longitudinal ridges called as "sand ribbons". Nezu and Nakagawa (1984) (hereafter, NN) investigated experimentally the turbulent structure of secondary flows. They used not an open water channel but a closed air conduit, in which the ridges were attached symmetrically on both top and bottom walls. This was because a better measurement accuracy of the secondary flows could be obtained with the use of the hot-wire anemometer in the air duct. Kawamura and Sumori (1999) (hereafter, KS) carried out a DNS of turbulent flow in a ridged channel with the same configuration as the experiment of NN. KS carried out the DNS on the condition that the pitch of the ridge was equal to the channel half width δ. They obtained a good agreement with the experimental results. In the actual river bed, however, the pitch of the ridge is known to be about 2δ. Accordingly, the present paper deals with the ridge wall with the pitch of 2δ.

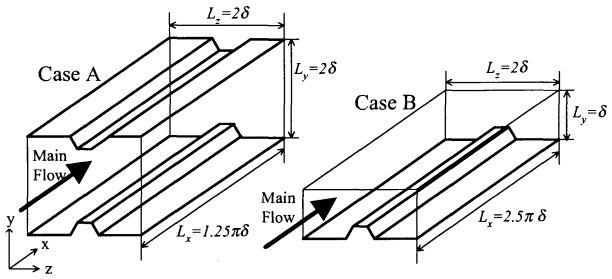

Figure 1 : Computational domain

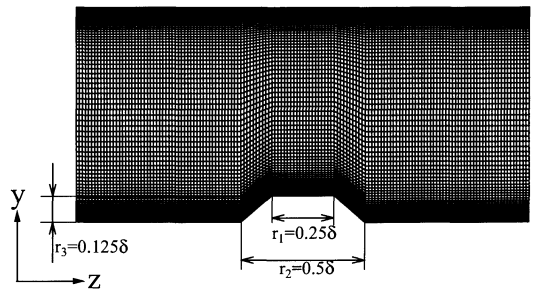

Figure 2 : Computational mesh

Two cases of DNS have been performed (see Figure 1). In the first one of Case A, the ridge elements were attached symmetrically onto both top and bottom walls in order to compare the results with the experiment by NN. In this case, the mid-height of the channel is a statistically symmetric plane but instantaneously not.

In the second case of Case B, we consider an open channel, that is, the ridge is attached only on the bottom surface and top is free, which is more similar to the actual river.

Various turbulence statistics such as mean the velocity distributions of streamwise, ver-

Table 1: Computational conditions

Case		A	B
Grid		Staggerd grid	
Coupling algorithm		Fractional step method	
Time advancement	Viscous terms	Crank-Nicolson method (y-direction)	
	Others	Adams-Bashforth method	
Spatial scheme	Convective terms	2nd-order Central scheme (Consistent)	
	Viscous terms	2nd-order Central scheme	
Boundary condition	x , z direction	Periodic	Periodic
	Upper wall	Non-slip	Free-slip
	Lower wall	Non-slip	Non-slip
Grid numger ($x \times y \times z$)		$48 \times 96 \times 72$	$192 \times 96 \times 144$
Computational volume		$1.25p\delta \times 2\delta \times 2\delta$	$2.5p\delta \times \delta \times 2d$
Spatial resolution	Δx^+	12.3	12.3
	Δy^+	$0.19 - 8.67$	$0.11 - 7.65$
	Δz^+	4.17	2.08
Time Step		$\Delta t = 0.0008\delta/u_\tau$	

Table 2: Conditions of NN's experiment and present DNS

		Re_τ	L_y	L_z	r_1	r_2	r_3	Geometry Field
Experimant (NN,1984)		582	2δ	2δ	0.25δ	0.5δ	0.125δ	air duct of ridged closed channel
Present	Case A	144	2δ	2δ	0.26δ	0.52δ	0.125δ	ridged closed channel
	Case B	146	δ	2δ	0.25δ	0.5δ	0.125δ	ridged open channel

tical and spanwise directions are obtained. A low speed streak over the ridge is captured by the conditional sampling and its structure is discussed.

NUMERICAL PROCEDURE

The governing equations for an incompressible flow transformed into the body-fitted coordinate system are given by
the continuity equation:

$$\frac{1}{J}\frac{\partial}{\partial \xi^k}\left(JU^k\right) = 0 \qquad (1)$$

and the Navier-Stokes equation:

$$\frac{\partial u_i}{\partial t} + \frac{1}{J}\left(JU^k\frac{\partial u_i}{\partial \xi^k}\right) = -\frac{\partial \xi^k}{\partial x_i}\frac{\partial p}{\partial xi^k} + \frac{1}{Re_\tau}\frac{1}{J}\frac{\partial}{\partial \xi^m}\left(g_{mk}\frac{\partial u_i}{\partial \xi^k}\right) + \delta_{i1}P_x \qquad (2)$$

where J is the Jacobian of coordinate transformation, U^k the contravariant velocity and g_{mk} the "mesh skewness tensor".

The generated grid is shown in Figure 2 for Case B, in which the top is a free surface where a rigid but free-slip surface is assumed.

Equations (1) and (2) are nondimensionalized by the channel width h and mean friction velocity $\langle u_\tau \rangle$ on the bottom wall. The Reynolds number Re_τ defined as $Re_\tau = \langle u_\tau \rangle \delta/\nu$ is approximately 144. This Reynolds number Re_τ is almost equal to the Reynolds number in the DNS of KS. The flow is driven by the mean pressure gradient P_x in the streamwise direction.

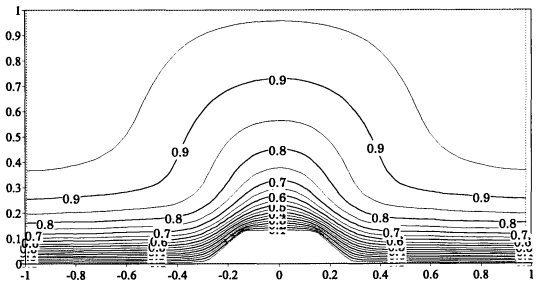

(a) Case A

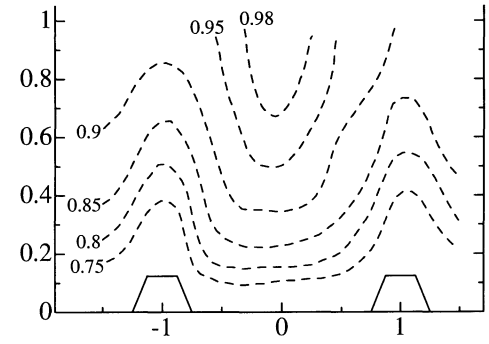

(b) NN'experiment

Figure 3 : Mean streamwise velocity contour

For the time integration, we employ the second-order Adams-Bashforth Method for convective terms and second-order Crank-Nicolson Method for the y direction in viscous terms. The convective terms in (2) are discretized by using the second-order consistent central scheme extended to the body-fitted coordinate system on the staggered grid. The turbulence statistics are obtained by averaging the flow field in the streamwise direction and in time. The computational conditions

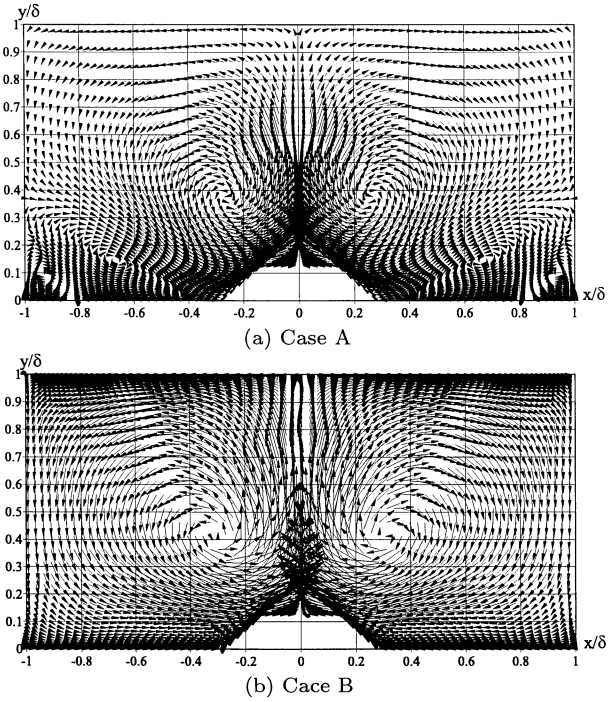

(a) Case A

(b) Cace B

Figure 4 : Mean secondary velocity vectors

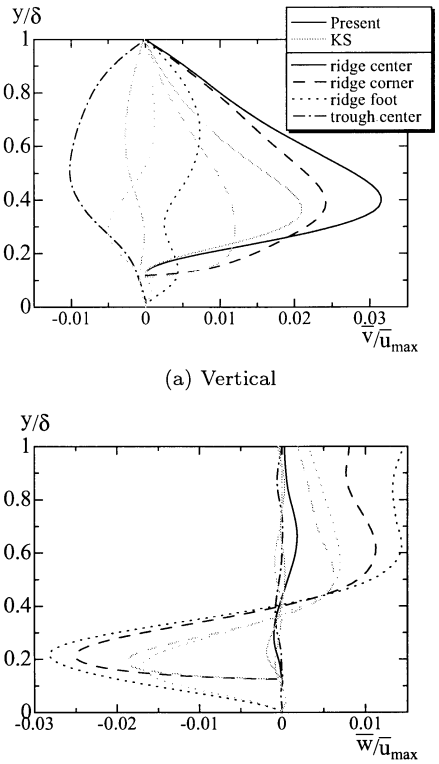

(a) Vertical

(b) Spanwise

Figure 5 : Mean velocity profiles

are given in Table 1. Table 2 compares the conditions of NN's experiment and the present DNS .

RESULTS

Four locations are specified to present the obtained results.

1. ridge center : $z/\delta = 0$
2. ridge corner : $z/\delta = 0.125$
3. ridge foot : $z/\delta = 0.25$
4. trough center: $z/\delta = 1.0$

Mean velocity

Figure 3a shows the contours of streamwise mean velocity in y-z plane. The contours are distorted by the ridge. The distortion becomes less eminent away from the wall. These results are in good agreement with experimental result obtained by NN (see Figure 3b), although both Reynolds numbers are rather different.

The mean secondary velocity vectors in $y-z$ plane are shown for Case A in Figure 4(a). The existence of a pair of nearly symmetrical streamwise vortices, which is called as the cellular secondary current, is observed in both sides of the ridge. The upflow occurs above the top of the ridge. The downflow takes place above the trough and flows obliquely towards the ridge foot. This induces two vertices, i.e. the one near the channel center and the other close to the trough surface. If the secondary flow of this type exists, it means that a once sedimented ridge would be destroyed by the secondary flow. For this reason, Case A cannot be a good simulation of the actual river.

Figure 4(b) shows the mean secondary velocity vector in $y-z$ plane for Case B. Similar to Case A, the cellular secondary current exits. In this case, however, the downflow impinges directly to the trough center wall. Accordingly, only one secondary vortex is induced in Case B.

For the sand ribbon to be sedimented, the direction of the secondary flow over the riverbed must be towards the ridge foot in average. Otherwise, even if a ridge were once sedimented, it would be destroyed. Thus, it can be concluded that the Case B, with an assumption of the free top surface, indeed simulates better the actual riverbed. This is due to a difference in the strength of the secondary velocity between in Cases A and B.

Figure 5 shows the distribution of the vertical and spanwise mean velocities at some selected spanwise locations. The secondary velocity of Case B is stronger than that of Case A. This can be explained as follows. The center plane of Case A is symmetric only statistically, that is, the instantaneous vertical flow can penetrate the center plane. On the other hand, in Case B, the top surface is a rigid free surface, thus the upward flow gives its energy to the span and streamwise components. The so-

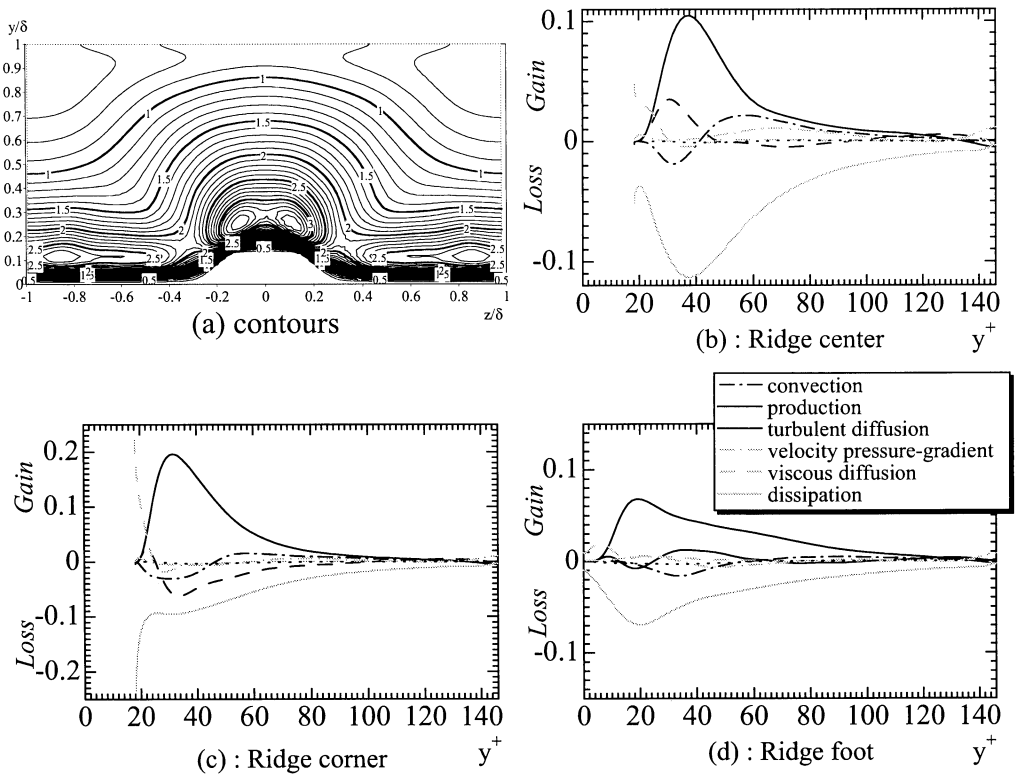

Figure 6 : Turbulent kinetic energy : (a) Contors ; (b),(c),(d) Budget along a vertical line

called splatting takes place. This causes the stronger spanwise flow in the free surface of Case B than in Case A. Thus the secondary cellular motion is more enhanced in Case B, As the result, the downward flow in the trough center penetrates down to the bottom surface.

Turbulent energy

Figure 6(a) shows countours of the turbulent kinetic energy. Its maximum peak exists not above the ridge center but above the ridge corner. The peak becomes minimum above the ridge foot.

The transformed of turbulent kinetic energy equation into the body-fitted coordinate system can be written as

$$\frac{\partial k}{\partial t} = C_k + P_k + T_k + \Pi_k + D_k - \varepsilon_k \qquad (3)$$

$$\begin{aligned} C_k &= -\frac{1}{J}\left(J\langle U^k\rangle \frac{\partial k}{\partial \xi^k}\right) \\ P_k &= -\frac{1}{J}\left(J\langle U'^k u_i'\rangle \frac{\partial \langle u_i\rangle}{\partial \xi^k}\right) \\ T_k &= -\frac{1}{J}\frac{\partial}{\partial \xi^k}\left(\frac{1}{2}J\langle U'^k u_i'^2\rangle\right) \\ \Pi_k &= -\frac{1}{\rho}\frac{\partial \xi^k}{\partial x_i}\langle u_i' \frac{\partial p'}{\partial \xi^k}\rangle \end{aligned}$$

$$\begin{aligned} D_k &= \frac{1}{J}\frac{\partial}{\partial \xi^k}\left(\nu J G^{km}\frac{\partial k}{\partial \xi^m}\right) \\ \varepsilon_k &= \frac{1}{J}\nu J G^{km}\left\langle \frac{\partial u_i'}{\partial \xi^k}\frac{\partial u_i'}{\partial \xi^m}\right\rangle \end{aligned}$$

Figures 6(b) $\sim$ (d) show the turbulent kinetic energy budget distribution at the three locations. Each term is normalized by the mean friction velocity. The maximum value of the production term is largest at the ridge corner and smallest at the ridge foot. This explains the distribution of the turbulent kinetic energy discussed above.

High and low speed flow streaks

Figure 7 shows the instantaneous velocity fields visualized for high and low speed streaks. The gray is the low speed region and the black is the high speed one. The streak emerges near the wall as in the plane channel flow. They appear more often around the ridge than over the trough.

The low speed region often rises up from the ridge top towards the free surface. When the strong upflow occurs, the low speed region over the wall reaches near the free surface. To capture its structure, the upward motion has been conditionally sampled. That is, the three velocity components are stored only when the

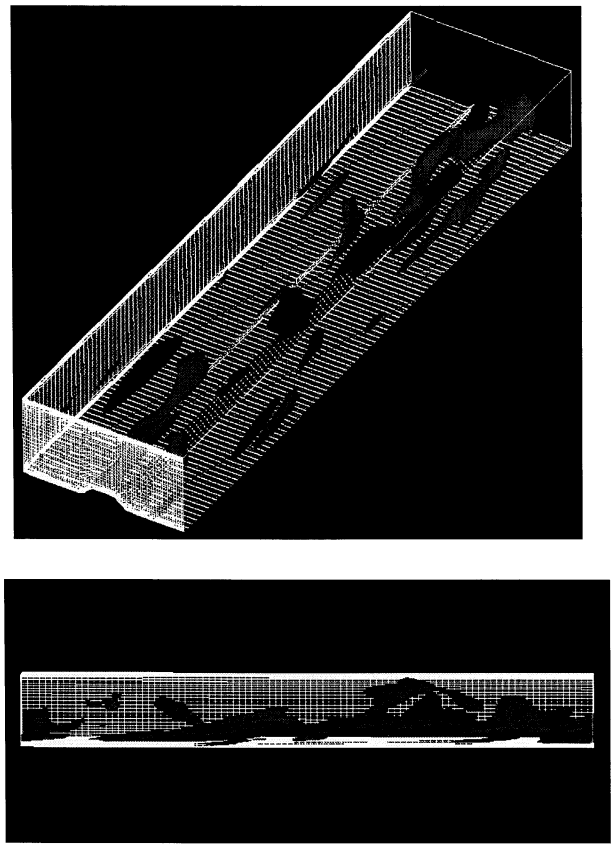

Figure 7 : High and low speed regions
(Black:$u'^{+} > 2.0$, Gray:$u'^{+} < -2.0$)

vertical velocity exceeds its ensemble average at a sampling point. A sampling point is assigned at above the ridge center and the mid height between the bottom wall and free surface (see Figure 8).

The obtained flow field is shown in Figure 9, where gray is the low speed region, black the high speed one. The low speed streak emerges above the ridge center and is accompanied by a pair of the high-speed streaks in its both sides. No other structure can be found than this one set of stresks. The side view of the low speed streak is illustrated in Figure 10. The sampling point is given by a cross in Figure 10. The figure indicates that the low speed region is first almost parallel to top of the ridge surface. From near the mid-height of the channel depth, however, it becomes obscure and rises almost vertically upwards. Four successive sections are shown in Figure 11, which confirms the above observations.

The conditionally sampled velocity field in the y-z plane is given in Figure 12, where the velocity vectors less than $u_{max} \times 10^{-3}$ eliminated to avoid the complication. Three vertical sections at (c)$x_0 - 0.64\delta$, (b)$x_0 - 0.32\delta$ and (a)x_0 are illustrated, where x_0 is the samplihg point. At the upstream of the sampling point in Figure 12(c), a pair of small vortices appear at the height of $y/\delta = 0.3$. The vortex pair then grows and rises up downstream up to $y/\delta = 0.5$ as seen in Figure 12(a).

The center of the vortex is located roughly at the mid-height of the channel depth. Accordingly, the upward flow is concentrated up to the mid-height and then diversified towards the free surface. This explains the reason why the low speed streak is confined in a narrow region at the mid-height of the channel and then suddenly rises almost vertically upwards from there.

Figure 13 shows a combination of the calculated second invariant and high and low speed regions. It emerges near the sampling point and rises up obliquely. The second invariant of the velocity gradient tensor, which is often used to detect the vortex region, is obtained from the conditionally averaged three dimensional velocity field. The detected vortex exists between the low and high speed regions. The front of the low speed region is wrapped by high value of the second invariant of velocity gradient tensor.

Figure 14 shows the component of streamwise(ω_x) and spanwise(ω_z) vorticity vectors, where the gray is ω_x and the white ω_z. The streamwise vortex ω_x takes place on the both sides of the ridge. It arises from the cellular secondary current. Near the samlping point, both streamwise vortices are rising up and tend to merge with each other. This phenomenon can be confirmed by a comparison with Figure 12. The spanwise vortex ω_z emerges above the ridge center near the sampling point. It rotates clockwise if observed from the positive z. The second invariant of velocity gradient tensor arises from this two vortices. The captured second invariant indicates a typical shape of the so-call horseshoe vortex.

ACKNOWLEDGEMENT

Computation of Case A was performed by Mr. T. Sumori, a former graduate student.

REFERENCES

Nezu, I. and Nakagawa, H.: Cellular secondary currents in straight conduit, *J. Hydraulic Eng., ASCE*, Vol.**110**, No.**2**, 173-193, (1984).

Kawamura, H. and Sumori, T.: DNS of turbulent flow in a channel with longitudinally ridged walls, *Direct and Large-Eddy Simulation III, P. R. Voke et al., Ed., Kluwer Academ. Pub.*, 405-416, (1999).

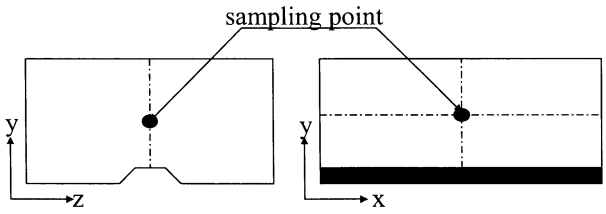

Figure 8 : Sampling point

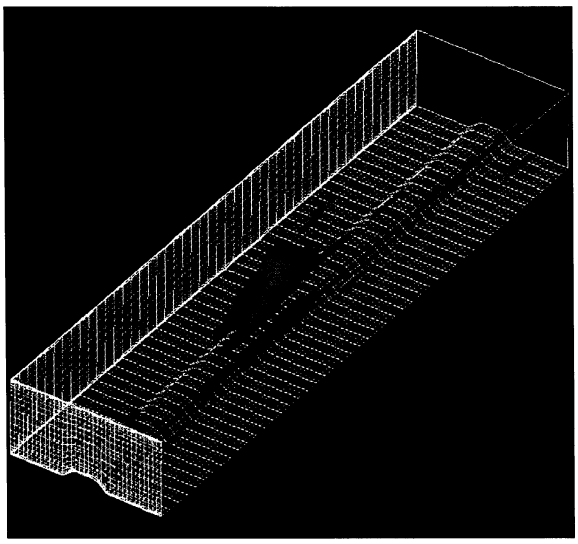

Figure 9 : Conditionally sampled high and low speed region

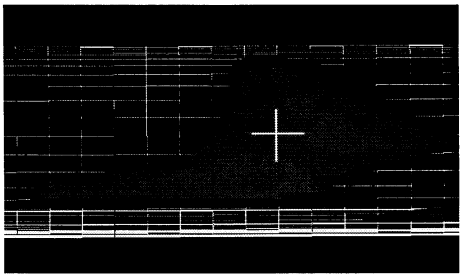

Figure 10 : Sideview of low speed region

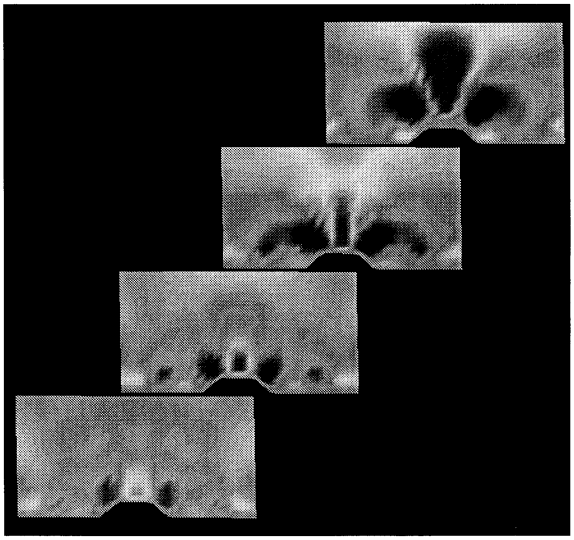

Figure 11 : Successive sections of conditionally sampled high and low speed contours

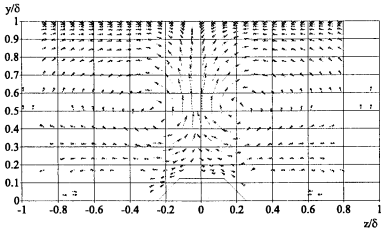

(a) $x = x_0$(at sampling point)

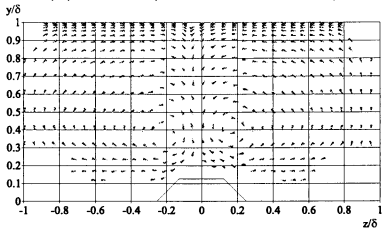

(b) $x = x_0 - 0.32\delta$

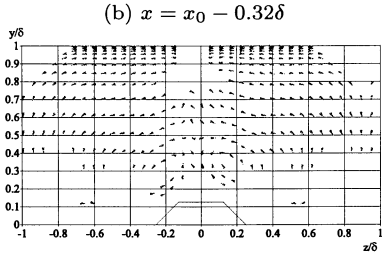

(c) $x = x_0 - 0.64\delta$

Figure 12 : Conditionally sampled secondary velocity vectors

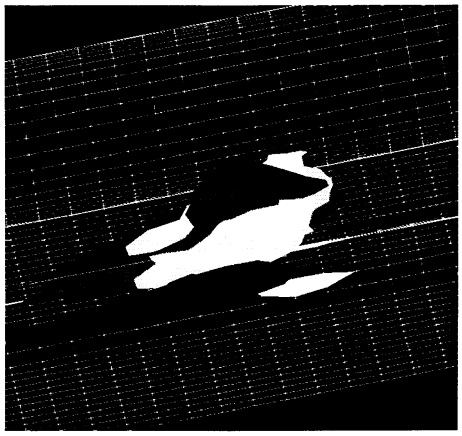

Figure 13 : A set of high and low speed streaks (Black is high speed streak, Gray is low speed streak) and second invariant of velocity gradient tensor (White)

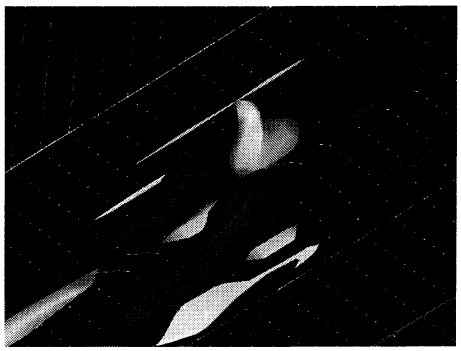

Figure 14 : Vorticity vector component (Gray:ω_x, White:ω_z)